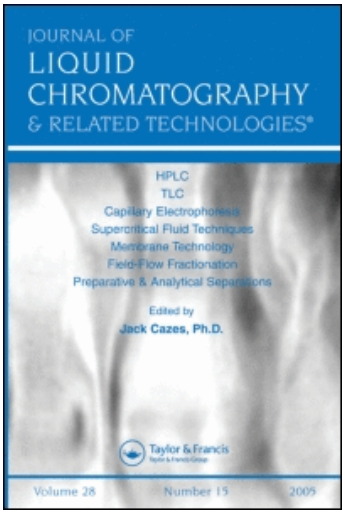

Journal of Liquid Chromatography & Related Technologies

Publication details, including instructions for authors and subscription information:
http://www.informaworld.com/smpp/title~content=t713597273

Experimental and Empirical Characterization of Reversed Phase Media

A. M. Katti[a]; C. Hopper[a]; N. E. Tarfulea[b]
[a] Department of Chemistry, Purdue University Calumet, Hammond, Indiana, USA [b] Department of Mathematics, Purdue University Calumet, Hammond, Indiana, USA

To cite this Article Katti, A. M. , Hopper, C. and Tarfulea, N. E.(2009) 'Experimental and Empirical Characterization of Reversed Phase Media', Journal of Liquid Chromatography & Related Technologies, 32: 3, 348 — 369
To link to this Article: DOI: 10.1080/10826070802631428
URL: http://dx.doi.org/10.1080/10826070802631428

Journal of Liquid Chromatography & Related Technologies®, 32: 348–369, 2009

ISSN: 1082-6076 print/1520-572X online
DOI: 10.1080/10826070802631428

Experimental and Empirical Characterization of Reversed Phase Media

A. M. Katti,[1] C. Hopper,[1] and N. E. Tarfulea[2]

[1]Department of Chemistry, Purdue University Calumet, Hammond, Indiana, USA
[2]Department of Mathematics, Purdue University Calumet, Hammond, Indiana, USA

Abstract: Characterization of solute, stationary phases, and mobile systems faces its challenges. This challenge touches on 5 characteristics studied herein. One, evaluate the effective particle diameter as a function of methanol–water composition. The objective is to use the effective particle size as measured by the pressure drop as a characteristic feature of the particle size for raw material testing. This is an alternative or improvement to using a characteristic of the particle size distribution. An effective particle diameter was measured at 3 microns for a nominal 5 micron material, indicative of a good particle size distribution. Two, quality parameters evaluated were precision, linearity, limit of detection, and limit of quantitation. Three, plate height data is measured as a function of flow rate in methanol-water with toluene as a probe solute. The data is evaluated by classic plate count models. Four, an improvement is made in the least square error, having a value of 10, for the van Deemter model by mathematical transformation of the reduced plate height and the reduced velocity of the raw data giving a 100 fold reduction in the error. Five, the mobile phase viscosity is characterized by application of the method of mathematical transformation of variables to enable determination of the viscosity, and then, calculation of the pressure drop as a function of temperature and composition with one equation and one set of parameters.

Keywords: Acceptance criteria, Effective particle diameter, Efficiency, Methanol, Model, Pressure drop, Quality control, Reduced velocity, Transformation, Van Deemter, Viscosity

Correspondence: A. M. Katti, Purdue Univerisity Calumet, Chemistry Department, Hammond, IN 46321, USA. E-mail: katti@att.net

INTRODUCTION

This paper shows the characterization of 5 properties in a reversed phase system. Characterization of the apparent particle size is reflective of the column pressure drop a characteristic of packed columns. The average particle size of chromatographic media is often determined from particle size distribution measurements. However, this method of particle size distribution measurement does not directly relate to the operating pressure or the column efficiency due to the effect of fines on the back pressure. For a non-uniform particle size distribution, it is difficult to calculate or predict the true operating pressure.

In process chromatography, the production rate is limited by the maximum pressure.[1] The value of the effective particle diameter has significant impact on the operating flow rate and the column efficiency, which in turn affects the cycle time, yield, and throughput. The effective particle size is useful for quality control and quantitation of the consistency of the virgin packing media, as well as for monitoring the degradation of a column with acceptance criteria for packing change. An evaluation of the effective particle diameter as a quality parameter is performed.

The description of pressure drop in packed beds lead to classic papers in the literature. The description of fluids flowing through open tubes under pressure, ΔP, the impact of shear stress and their relationship to the velocity was first deduced by Hagen[2] and independently by Poiseuille,[3] according to Equation (1) for Laminar flow in open tubes. The pioneering work of Darcy, Darcy's Law, originally characterized fluid flow through packed beds and developed a mathematical expression for the pressure drop.[4] The classic work of Ergun investigated pressure drop of gasses in packed columns to determine particle density.[5]

$$\Delta P = 15 \times \frac{u_{(\mathrm{cm/s})} \times L_{(\mathrm{cm})} \times \eta_{(\mathrm{cP})}}{d^2_{p(\mu\mathrm{m})^2}} \tag{1}$$

The quantity of experimental and theoretical papers on pressure drop are too many to review. This work references classic papers on the calculation of the pressure drop in columns packed with large particle sizes,[6] evaluation of viscous dissipation in chromatography columns,[7] relationships between pressure, diffusivity, and viscosity on irregular silica particles,[8] determination of the relationship between pressure drop, column length, and particle size,[9] and the relationship of pressure drop in parallelepiped[10] shaped particles. The characterization of fluid flow as laminar or turbulent in open tubes was originally defined by Reynolds as the ratio of inertial to friction forces.[11] Chromatography operates in laminar flow at a low Reynolds number as interpreted in the case of flow

over porous spherical particles packed in a cylindrical bed.[12] Under ideal conditions, the mobile phase and particles are incompressible; moreover, the particles are uniform in diameter and shape.

Another characteristic of reversed phase systems is the plate height relationship. The fundamental work of Van Deemter combined the plate and rate theory to identify terms that contribute to longitudinal eddy diffusion, longitudinal molecular diffusion, and resistance to mass transfer, which were found to be additive and that mass transfer kinetics are reasonably fast in many situations.[13] Before this work, the rate theory provided, in principle, information on kinetic phenomenon; however, there was no physical concept behind the phenomenon.[14] Until Van Deemter, the plate theory conceived the column as a number of stages or plates, which is an empirical method that had limited delineation of the mechanisms of band broadening.[15]

Subsequently, many other plate models have been developed. Golay derived a plate height equation for gas-liquid chromatography in open tubular columns where axial molecular diffusion, radial diffusion due to the laminar flow profile and excludes an eddy diffusion term.[16] The Golay equation is predictive because the parameters can be measured or estimated independently of the chromatographic result, and it has been shown to give excellent agreement with experimental results as demonstrated in both gas and liquid chromatography; although, this kind of column design is not practical for analytical or preparative separations.[17–19] Giddings expanded on the Van Deemter equation by including radial diffusion.[20] Horváth and Lin limited axial dispersion to the fluid around a thin stagnant film around each particle and derived an expression for the axial dispersion coefficient.[21] At high reduced velocities, Horváth and Lin show their expression to simplify the Knox empirical equation.[22] With these plate models, although their physical interpretation and derivation are different, it is very difficult to differentiate between them unambiguously unless data is collected over a wide range of velocities.[23]

These classic models trace the physical meaning of the terms and the parameters to fundamental phenomenon, though they are often used as empirical functions in practical applications. In this work, transformation of the variables was found to reduce the least square fitting errors. By inverting the transformation, the physical meaning of the model form is preserved. For the optimization of preparative chromatography via mathematical tools to an objective function, a continuous relationship is required between the plate count and the flow rate. The accuracy of this relationship effects the location of the true optimum.

Beyond the practical applications, the non-linearity of the plate height equations creates a natural driving force to seek a means to flatten,

mathematically, this curve in order to reduce the least square error upon curve fitting. A theoretical analysis is performed by transformation of variables in order to evaluate and find other forms of the plate height equation that minimize the error.

Validation of analytical methods and processes is a large area of study with books, guidelines from the International Conference on Harmonization, and the Food and Drug Administration detailing the definitions and procedures.[24–28] Evaluation of precision, accuracy, linearity, limit of detection, limit of quantitation, and providing acceptance criteria is one aspect of validation.

Characterization of the mobile phase regarding the viscosity as a function of temperature and composition has important implications for the operating pressure, the separation, and retention in chromatography.[29–32] The viscosity for chromatographic mobile phases is typically a strong, nonlinear function of temperature and composition. The modeling of viscosity as a function of temperature is commonly performed by a fit to the Antoine Equation.[33] Binary mixtures of viscosity have been modeled using the sum of the mole fraction and the natural log of the pure component viscosity product.[34] In some models an excess term is used and other times it is ignored returning to the original Arrhenius Equation.[35] For polar mixtures, Li and Carr[36] have used the Lobe Correlation to predict viscosity as a function of composition as a curve with different coefficients at each temperature. A recent comprehensive review of viscosity measurements and models is written.[37] The modeling of viscosity as a function of composition temperature as a surface for polar molecules that exhibit a high degree of hydrogen bonding is limited at best. Surface modeling or 3-D modeling of viscosity as a surface function for classic chromatographic systems is new.

Experimental viscosity data for methanol-water mixtures are complex due to the volume reduction upon mixing.[38] In a recent study, the value of the maximum viscosity and the composition at the maximum viscosity both increase with increasing carbon number.[39] As the number of carbon atoms increases beyond three, the trends become more complex due to limited solubility. Yet, functionalization of the pressure drop and the viscosity relationship with constant values of the parameters is fundamental to creating a mathematical expression for gradient applications, particularly in process chromatography where pressure limitations determine the operating parameters during optimization.[40,41] Optimization of the production rate to an objective function[42,43] requires a relationship between the plate height and the flow rate to determine the operating parameters (e.g. flow rate, temperature, load, particle size), cycle time, purity, and yield with known design parameters (e.g. column length, mobile phase composition, pressure maximum, feed composition, feed viscosity).

The advances in this paper focuses on (1) evaluation of the effective particle size as a quality parameter for packing media, (2) transformation of classical plate height models to an empirical model with a significant reduction in error, and (3) development of a mathematical function to model viscosity as a function of composition and temperature.

EXPERIMENTAL

An HP-1090 using Windows based Chemstation software (GMI Analytical, Ramsey, MN, USA) was used in the study. The pressure drop experiments used methanol (HPLC grade, Mallinckrodt, St. Louis, MO, USA) and de-ionized water v/v%. The plate height measurements used ACS grade toluene (Mallinckrodt, St. Louis, MO, USA) as the solute. Measurements were performed on columns: 4.6 mm × 50 mm Daiso SP-ODS-A, 5 μm, 120Å (Santa Clara, CA, USA), 4.6 mm × 50 mm Water's Symmetry, C18, 5 μm, 120Å (Milford, CT, USA), and a 10 mm × 250 mm Eka Nobel (Bohus, Sweden, USA), Si, 10 μm, 100 Å. Digitization of graphical data (Un-Scan-It® Orem, UT, USA).

RESULTS AND DISCUSSION

Quality Parameters

Pressure Drop Linearity

The pressure drop is measured over a range of flow rates and the methanol composition range. The pressure drop is calculated from Equation (1). The linear relationship observed in Figure 1 demonstrates the particles characterized are not compressible. Furthermore, the square plot indicates the pressure drop relationship is ideal according to Darcy's Law as the data follows the diagonal.

Effective Particle Size

Figure 2 illustrates the effective particle size range based on the measured pressure as a function of flow rate over the entire range of the methanol-water composition and 2 temperatures. The effective particle size is calculated based on Equation (1) from the measured pressure drop and dead time, as well as known values for the viscosity and column length. The mean effective particle size determined was in the range 2.4–3.2 micron and the reported nominal size was 5 micron. This consistency in the estimated and nominal particle size represents the tight distribution of the particle diameter

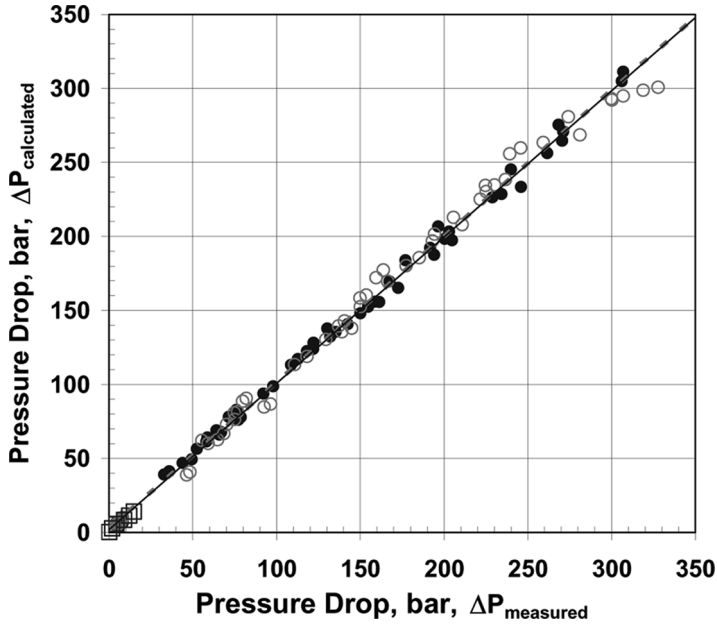

Figure 1. A square plot of the measured and predicted pressure drop. Column: Daiso (●), Waters (◯) and Eka Nobel (□). $F_v = 0.1, 1, 2, 3, 4$ mL/min. Reversed phase: 40(●), 60°C (◯). Normal phase: 60°C (□), 100% ethyl acetate, 40°C.

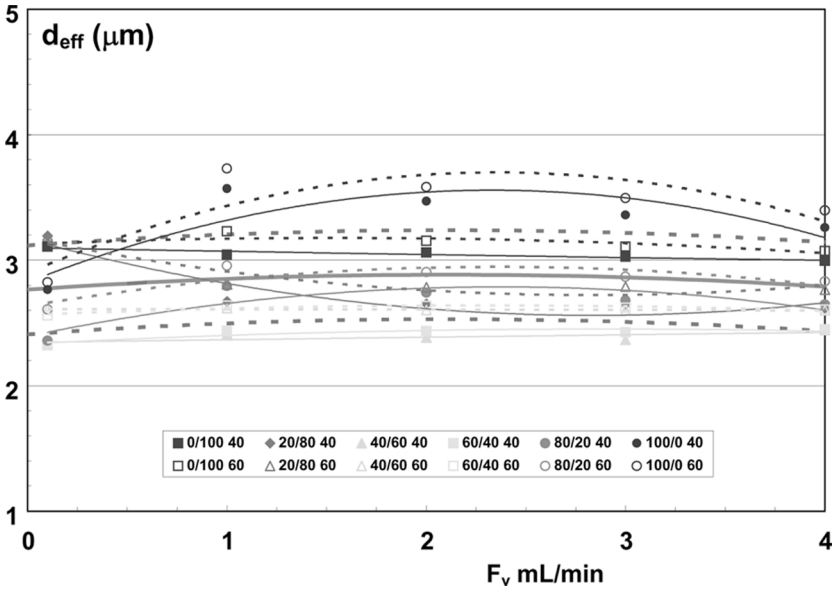

Figure 2. Plot of the effective particle size versus flow rate and methanol composition and temperature.

based on direct hydrodynamic measurements versus particle size distribution measurements. The lower effective particle size is likely due to a greater contribution of the pressure drop to due smaller diameter particles.

Limits of Detection and Quantitation

Figure 3 illustrates the calibration curve of toluene used to determine the limit of detection (LOD) and the limit of quantitation (LOQ). Equations (2) and (3) give values of 0.00239 v/v% and 0.00796 v/v%, respectively, where s_x and m are the standard deviation of the blank and the slope of the calibration curve, respectively.

$$LOD = \frac{3s_x}{m} \tag{2}$$

$$LOQ = \frac{10s_x}{m} \tag{3}$$

Linearity

Linearity was tested in the range 0.002 to 2 v/v% (Figure 4). Evaluation of a linear equation across the entire experimental results gives a correlation coefficient of 0.9780, and this value is understood by the systematic over estimation of the data in the lower concentration range and

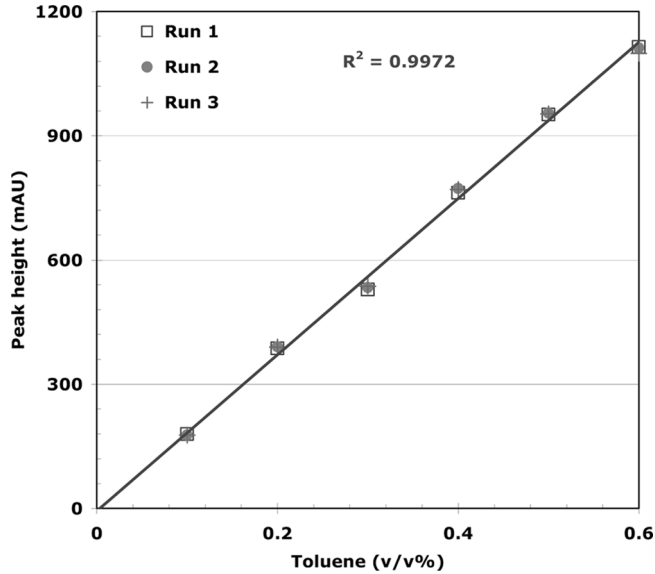

Figure 3. Calibration curve for determination of LOD and LOQ.

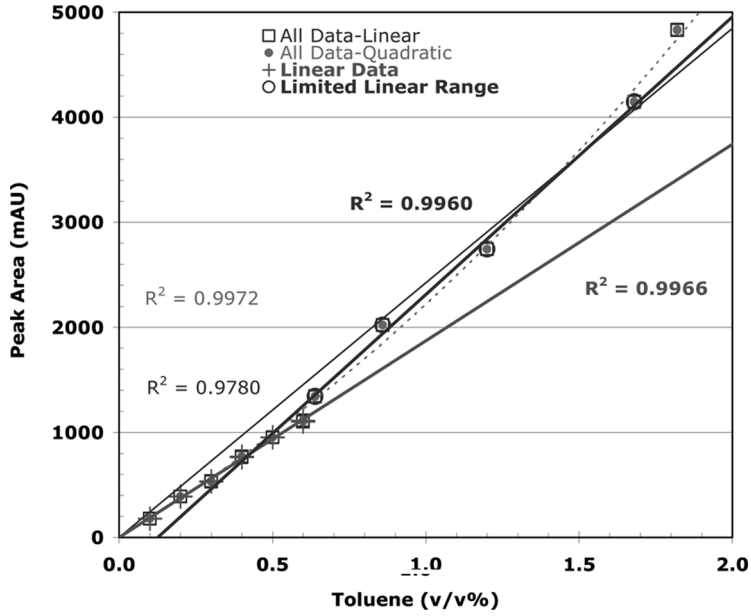

Figure 4. Calibration curve for determination of linearity.

underestimation of the data in the higher concentration range. In addition, the lack of linearity is exhibited in the correlation coefficient of a quadratic fit having a value of 0.9972. There are regions of linearity. For example, a tangent line going through the origin over a concentration range ≤ 0.7 v/v% gives a correlation coefficient of 0.9966 and the range 0.6–1.7 v/v%, has a correlation coefficient of 0.9966.

Precision

The day to day precision is 0.34% and 0.24% per cent relative standard deviation for toluene and naphthalene, respectively. The F-test result at 95% confidence indicted the precision for each day was statistically equal for both compounds, Table 1.

Table 1. Day 1 versus day 2 precision

Compound	Day	k′	RSD (%)	Equal?
Toluene	Day 1	2.99	0.25	Y
	Day 2	2.98	0.35	
Naphthalene	Day 1	4.207	0.14	Y
	Day 2	4.214	0.22	

Plate Count Relationships

Plate count data for toluene was measured in triplicate over a temperature range of 40–60°C, 0–100% methanol, and flow rates between 0.1 and 5 mL/min using the width at half height method, Figure 5. The plate count results was non-dimensionalized to the reduced plate height, $h = L/(Nd_p)$, and the flow rate to the reduced velocity ($\nu = ud_p/D_m$) where u is the linear velocity, d_p is the particle size, and D_m is the molecular diffusion coefficient. The diffusion coefficient used was a fixed value, an average over the range obtained using the Wilke-Chang equation, using as solvent the weighted average parameters. This gives a similar value measured by Li and Carr for the average molecular diffusion coefficient. Due to the paucity of data and the errors in both the Schiebel[44] and Wilke-Chang correlations, this simplification was viewed justifiable.

Figure 6 illustrates Van Deemter model using a least square fitting algorithm and the data. Figure 7 illustrates the residuals at each reduced velocity. Note, the greatest source of error is at very low values of the reduced velocity. In order to consolidate the mathematical function of the various plate models for comparison, Equation (4), a generalized model was applied.

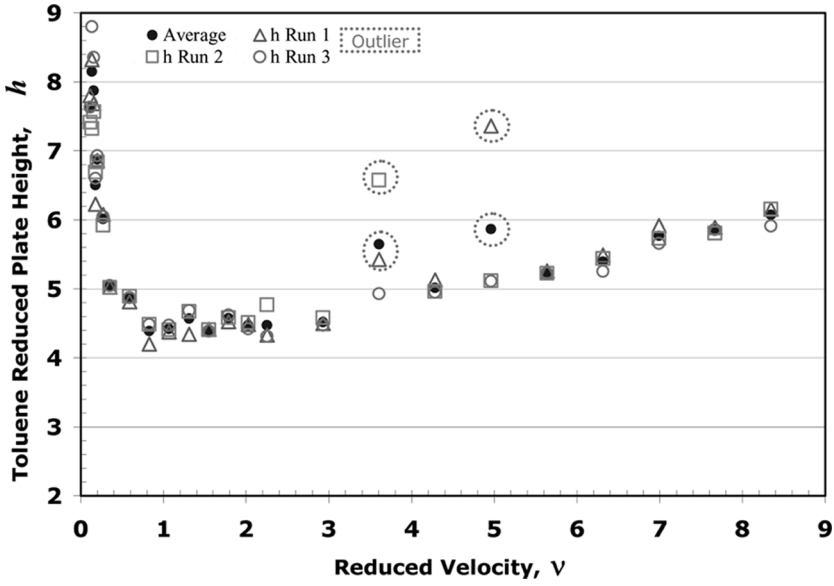

Figure 5. Reduced plate height versus reduced velocity data: Run 1 (△), Run 2 (□), Run 3 (◯), Average (●), outliers (dotted circles).

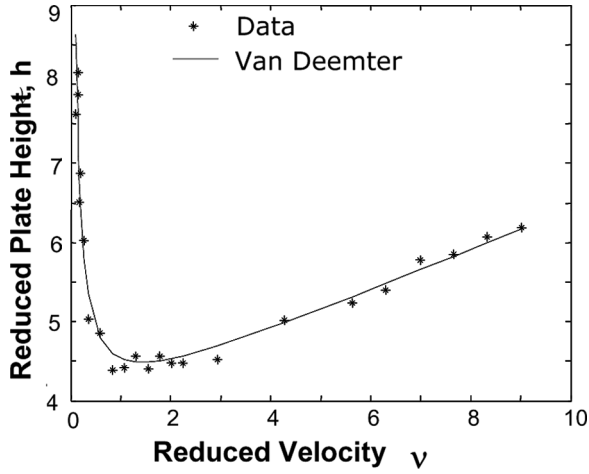

Figure 6. Least square fit of Van Deemter model. Data (*) Van Deemter (—).

$$h(\nu) = B/\nu + C\nu + A \cdot f(\nu) \tag{4}$$

Table 2 summarizes the function $f(\nu)$ for the Golay, Van Deemter, Knox, and Universal models,[45] where the data was applied to an unconstrained nonlinear optimization technique, the Nelder-Mead simplex algorithm.[46] This algorithm minimizes a scalar valued nonlinear function of n real variables using only the values of the function, without

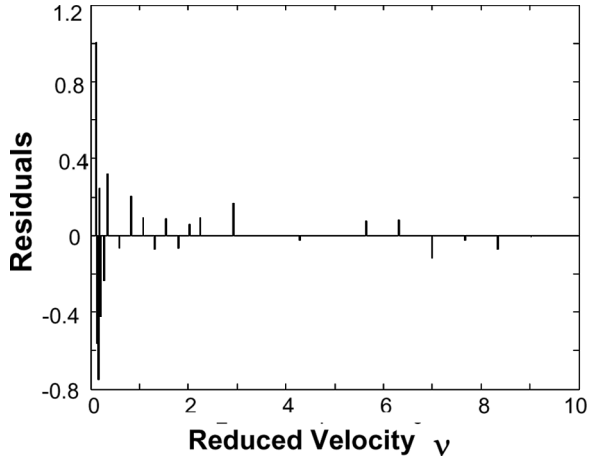

Figure 7. Histogram of the residuals of Van Deemter model.

Table 2. Summary of general mathematical function

Name	Model	$f(\nu)$
Golay	$h(\nu) = B/\nu + C\nu$	0
Van Deemter	$h(\nu) = B/\nu + C\nu + A$	1
Knox	$h(\nu) = B/\nu + C\nu + A\nu^{1/3}$	$\nu^{1/3}$
Universal	$h(\nu) = B/\nu + C\nu + A/(1 + w\nu^{-n})$	$1/(1 + w\nu^{-n})$

any implicit or explicit information on the derivative.[47] The objective function applied was the error by the least square technique.

For each model, Table 3 summarizes the values of the coefficients, the error, and the residuals. The Golay model exhibited the highest value of the error, 67, which is an order of magnitude greater than the other models. Although the physical meaning of the Golay model comes from capillary columns, its functional form is used for curve fitting of packed bed columns. The Knox Model gives a value of the error, 7, a significant reduction; however, the value for C, 5.32E-11, is essentially zero. This result shows for this data that the Knox model becomes degenerate.

The Van Deemter and Universal models, have the smallest and same value of the error, 2.4. This is because the value of the parameter n in the Universal model is 3.83E-11, essentially zero. At $n = 0$ the Universal model simplifies to the Van Deemter model. Therefore, the simplest model giving the least error with respect to the data is the Van Deemter model. The function $f(\nu)$ in Equation (4) is constant for the Golay and Van Deemter models, a power function of exponent $1/3$ for the Knox model and a Hill type function, Equation (5), for the Universal model.

$$f(\nu) = \frac{\nu^n}{\nu^n + w} \tag{5}$$

Since the Universal model simplifies to the Van Deemter model and the Knox model degenerates with a fixed exponent to ν and $C \approx 0$, this investigation of models is extended by considering a more general case

Table 3. Summary of model coefficients, error and residuals – non transformed

Model Name	A	B	C	w	n	Error	Residuals
Golay	1.173	0.860	–	–	–	66.6	−17.2
Van Deemter	3.732	0.535	0.264	–	–	2.429	1.68e-4
Knox	3.064	0.877	5.32e-11	–	–	7.44	−1.95
Universal	5.062	0.535	0.264	0.356	3.83e-11	2.429	−7.47e-5

Table 4. Summary of generalized model coefficients – non transformed

Description	*A*	*B*	*C*	*N*	Error	Residuals
Nonnegative *N*	3.732	0.535	0.264	2.571e-10	2.429	2.166e-04
Unconstrained *N*	3.846	0.327	0.390	−0.149	2.109	−0.005

where $f(\nu) = \nu^N$ presented in Equation (6).

$$h(\nu) = \frac{B}{\nu} + C\nu + A\nu^N \tag{6}$$

Evaluation of Equation (6) suggests that N may be a non-negative value or an unconstrained real number. These two cases are evaluated in the minimization process. When N is constrained to a non-negative value, $N = 2.571\text{E-}10$ or ≈ 0. Thus, Equation (6) transforms to the Van Deemter model with exactly the same coefficients as in Table 3. When N is unconstrained, $N = -0.149$; however, the differences, $|h_{nonnegative}(\nu) - h_{unconstrained}(\nu)|$, corresponding to the two cases range $[10^{-4}, 10^{-1}]$. This implies no significant differences between the non-negative and unconstrained value of N models.

A second approach to reducing the error is to transform the data using well defined, continuous functions. Then, these transformed functions can be qualitative analyzed and compared with the models in Table 2. Due to the nature of the steep diffusion drive slope and the change in slope, several standard transformations were examined (e.g. power, exponential, logarithmic, rational functions), as well as paired combinations of these functions. Fourier transformations or trigonometric functions are not applicable for this asymmetrical saddle type surface. Among these, two functions improve the error and the residuals in the minimization process: the square root and the logarithmic function.

An analysis based on the following function pair transformations of h and ν is performed: (i) $\sqrt{h}$ versus $\sqrt{\nu}$, (ii) $\log(h)$ versus ν, and (iii) $\log(h)$ versus $\sqrt{\nu}$. For one transformation, each of the 4 models is evaluated. Table 5 summarizes the transformed equation $y = h(\nu)$ as $\sqrt{h}$ versus $\sqrt{\nu}$,

Table 5. Summary of mathematical functions—transformation (i)

Model Name	Transformation Function
Golay	$h(x) = \left(\frac{B}{x} + Cx\right)^2$
Van Deemter	$h(x) = \left(\frac{B}{x} + Cx + A\right)^2$
Knox	$h(x) = \left(\frac{B}{x} + Cx + Ax^{1/3}\right)^2$
Universal	$h(x) = \left(\frac{B}{x} + Cx + \frac{A}{1+wx^{-n}}\right)^2$

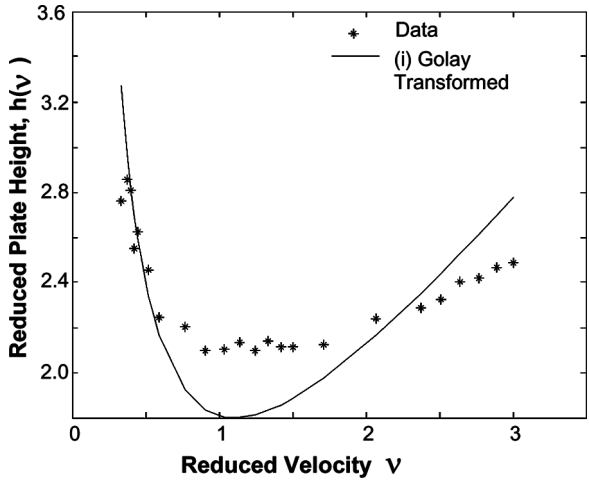

Figure 8. Transformed $\sqrt{h}$ versus $\sqrt{\nu}$ Golay model. Data (*) Golay (—).

where it takes the form $y = (h(\sqrt{\nu}))^2$ for each model. Visualization of these empirical fits to the experimental data is illustrated for the Golay, Knox, Van Deemter, Universal, in Figures 8–11, respectively. The visual distinction between Knox, Van Deemter, and Universal is unclear and requires quantitative interpretation. For one model, each of the transformations is evaluated. Table 6 summarizes the Van Deemter model

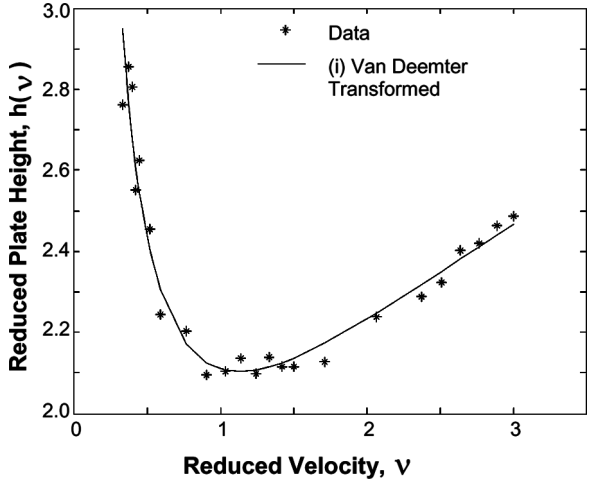

Figure 9. Transformed $\sqrt{h}$ versus $\sqrt{\nu}$ Van Deemter model. Data (*) Van Deemter (—).

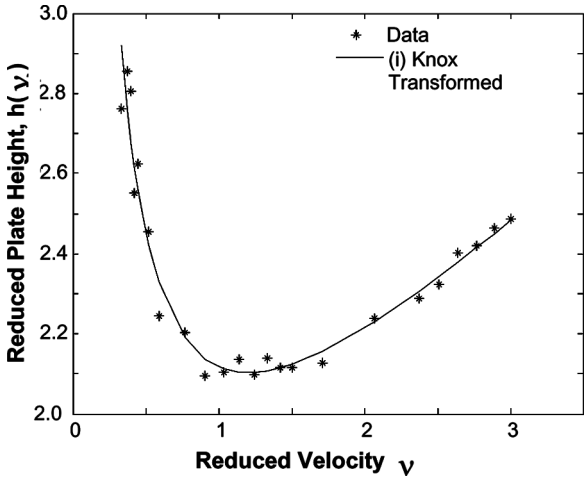

Figure 10. Transformed $\sqrt{h}$ versus $\sqrt{\nu}$ Knox model. Data (*) Knox (—).

transformed with mathematical functions (i)–(iii). A quantitative analysis for the 4 models with each transformation pair (i)–(iii) was compared by determination of the transformed model coefficients, the value of the error, and the residuals in Tables 7–9.

Tables 7–9 show the greatest error is obtained using the Golay model; however, the error has been reduced 2 orders of magnitude from 67 untransformed to 0.5 in transformation (iii). Similarly, the Van Deemter and Knox models showed a 2 order of reduction in error from

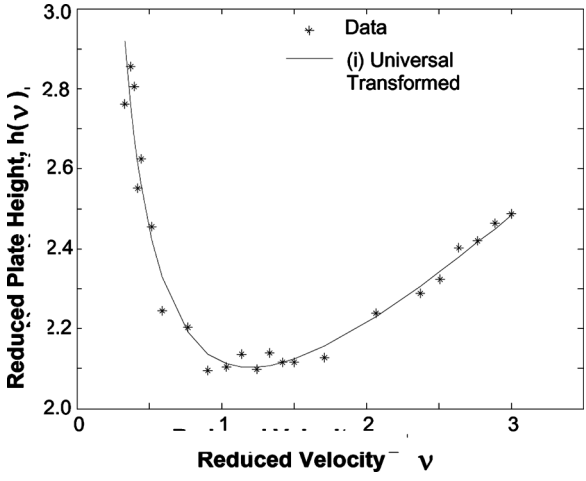

Figure 11. Transformed $\sqrt{h}$ versus $\sqrt{\nu}$ Universal model. Data (*) Universal (—).

Table 6. Summary of the transformed van deemter models

Transformation	Van Deemter Expression	Case #
h vs ν	$h(v) = \frac{B}{\nu} + C\nu + A$	(0)
$\sqrt{h}$ vs $\sqrt{\nu}$	$h(\sqrt{\nu}) = \left(\frac{B}{\sqrt{\nu}} + C\sqrt{\nu} + A\right)^2$	(i)
$\log(h)$ vs ν	$h(\nu) = \exp\left(\frac{B}{\nu} + C\nu + A\right)$	(ii)
$\log(h)$ vs $\sqrt{\nu}$	$h(\sqrt{\nu}) = \exp\left(\frac{B}{\sqrt{\nu}} + C\sqrt{\nu} + A\right)$	(iii)

Table 7. Comparison of models: (i)$\sqrt{h}$ versus $\sqrt{\nu}$

(*i*) $\sqrt{h}$ vs $\sqrt{\nu}$	*A*	*B*	*C*	*W*	*N*	Error	Residuals
Golay	1.00	0.81	–	–	–	1.20	−17.20
Van Deemter	1.250	0.514	0.354	–	–	0.073	−1.960e-4
Knox	1.360	0.655	0.0952	–	–	0.084	−0.006
Universal	1.250	0.514	0.354	5.353e-12	0.306	0.074	4.292e-6

Table 8. Comparison of models: (ii) log(h) vs ν

(ii) Log(*h*) vs ν	*A*	*B*	*C*	*w*	*n*	Error	Residuals
Golay	0.326	0.268	–	–	–	8.78	−6.33
Van Deemter	1.374	0.091	0.049			0.0705	−4.66e-4
Knox	0.982	0.231	9.34e-10	–	–	1.19	−1.00
Universal	1.374	0.0911	0.487	0.383	2.41e-10	0.0705	−1.07e-4

Table 9. Comparison of models: (iii) log(h) vs $\sqrt{\nu}$

(iii) Log(*h*) vs $\sqrt{\nu}$	*A*	*B*	*C*	*w*	*n*	Error	Residuals
Golay	0.727	0.586	–	–	–	0.476	−0.555
Van Deemter	0.773	0.429	0.301	–	–	0.0482	1.52e-4
Knox	0.839	0.517	0.142	–	–	0.055	−0.0049
Universal	0.773	0.429	0.301	0.707	1.30e-9	0.0482	5.05e-6

Table 10. Comparison of transformations for the van deemter model

Function	Case #	*A*	*B*	*C*	Error	Residuals
h vs ν		3.7318	0.5349	0.2638	2.4286	−1.6809e-4
$\sqrt{h}$ vs $\sqrt{\nu}$	(i)	1.2500	0.5144	0.3538	0.0734	−1.9595e-4
$\log(h)$ vs ν	(ii)	1.3741	0.0911	0.0486	0.0705	−4.6604e-4
$\log(h)$ vs $\sqrt{\nu}$	(iii)	0.7731	0.4291	0.3011	0.0482	1.5222e-4

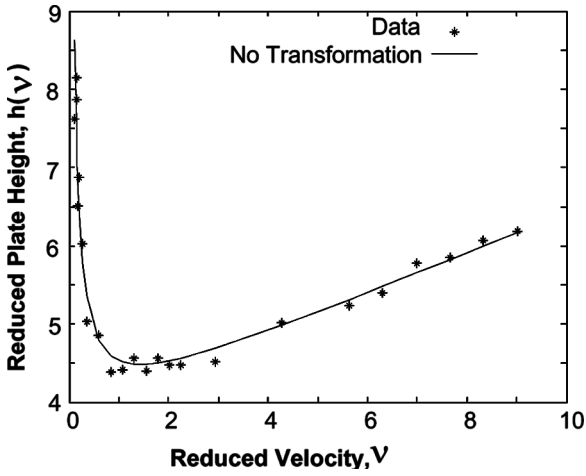

Figure 12. Untransformed Van Deemter model. Data (*) Van Deemter (—).

2.4 untransformed to 0.04 in transformation (iii). Lastly, the Knox model exhibits the same trend with a 2 order magnitude reduction in error by the use of transformation (iii) to an error value of 0.05. Whether transformed or untransformed, errors reduce from the Golay to the Knox to the Universal and Van Deemter models giving the lowest error. Similarly, the transformed expression of the Universal model degenerates to the Van Deemter model and has the same values for

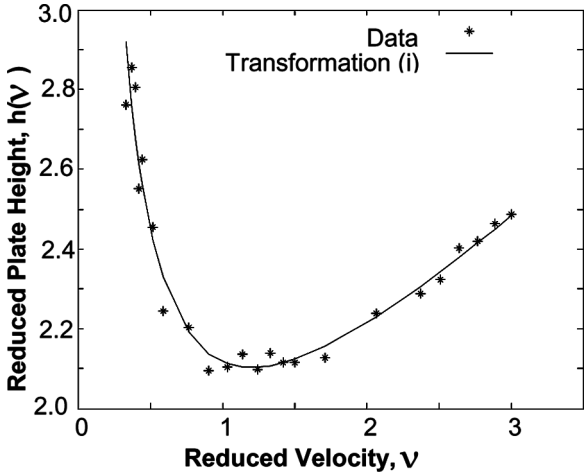

Figure 13. Transformed Van Deemter model $\sqrt{h}$ vs $\sqrt{\nu}$. Data (*) Van Deemter (—).

their coefficients. Note, the reason for this degeneration may differ and may not necessarily be because $w \approx 0$. In all models, transformation iii gave the least error.

Transformation (i)–(iii) performed on the general model, Equation (8), with nonnegative N or unconstrained N result in a value of N that is approximately zero, reducing to the Van Deemter model. Similar to the untransformed results, the transformed Van Deemter model gives the lowest residuals. In all transformations, the Van Deemter model gave a substantially lower error. Following the mathematical transformations in Table 6, Figures 12–15 illustrate the fit of these transformations of the Van Deemter model and the data. Without quantitative analysis in Tables 7–9, it would be difficult to select the transformation with the least error.

Contrasting the residuals for the functions giving the lowest and highest error, Figures 16 and 17 compare the Van Deemter equation transformation (iii) and the untransformed Golay. The individual residual can be up to 1 or 2 orders of magnitude apart. However, the sum of the residuals is 1.5E-4 versus -17 for these models, respectively.

Viscosity

In order to create a uniform expression to estimate the pressure drop in reversed phase chromatography a multidimensional model is required. The relationship between viscosity, composition, and temperature is a 3-D relationship that can be integrated into one model with fixed values

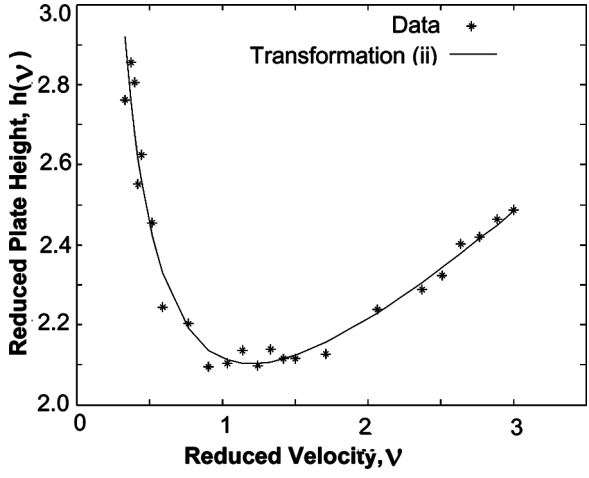

Figure 14. Transformed Van Deemter log(h) vs ν. Data (*) Van Deemter (—).

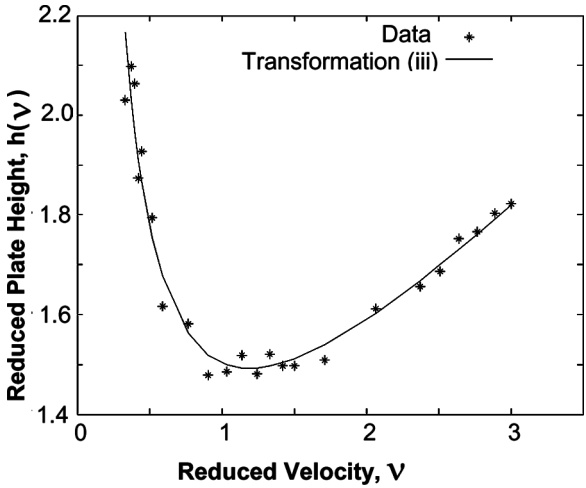

Figure 15. Transformed Van Deemter log(h) vs $\sqrt{\nu}$. Data (*) Van Deemter (—).

of the coefficients. The nature of the problem is visualized in Figure 18, where the viscosity is plotted as a function of the composition and temperature. Fitting this kind of surface function in two dimensions is difficult, because of the asymmetry observed along the parallel planes x-T and η-T. Use of Equation (7) to create a surface gives an error of

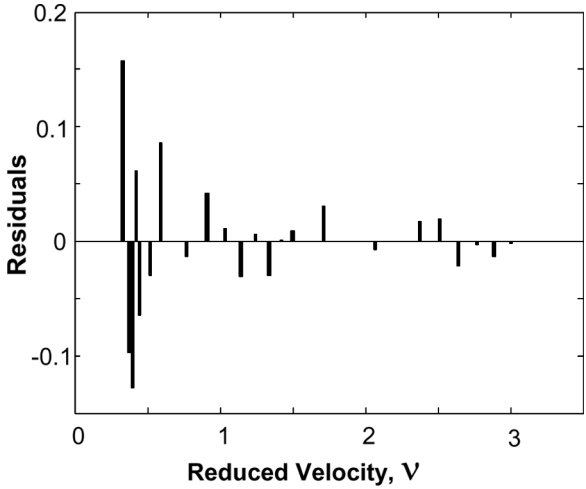

Figure 16. Histogram of residuals for Van Deemter transformation (III), log(h) vs ν.

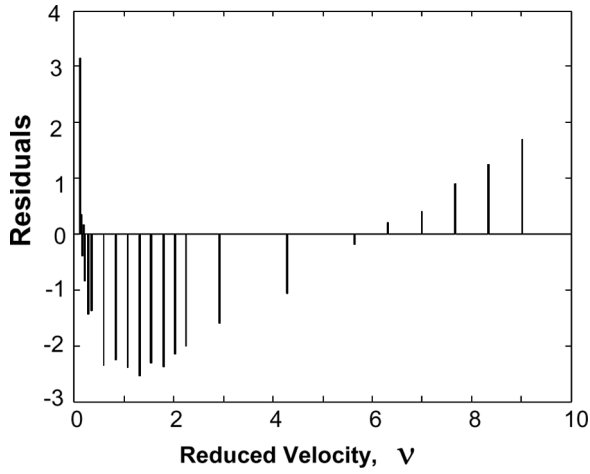

Figure 17. Histogram of residuals for untransformed Golay model.

10, Figure 19. Due to the highly nonlinear surface, this fitting of the data is difficult and requires transformation to flatten the curve.

$$\eta(x, T) = a(a_1 e^{-a_2 T} + a_3)(b_1 x^2 + b_2 x + b_3) \tag{7}$$

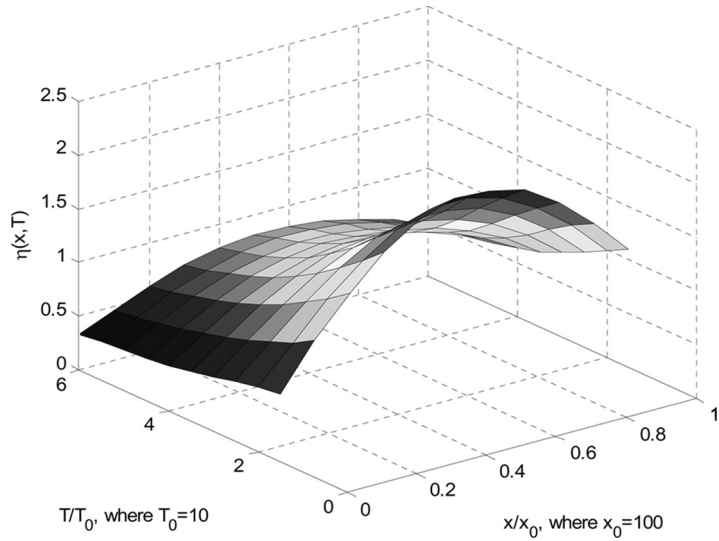

Figure 18. The viscosity versus composition and temperature surface with experimental data.

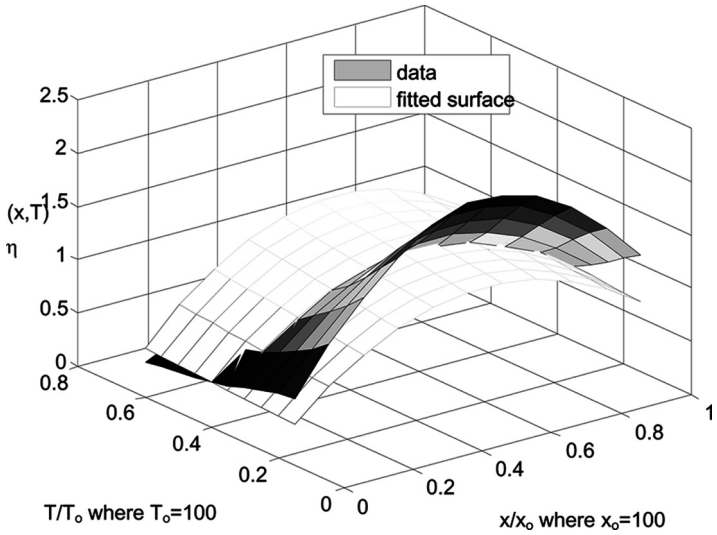

Figure 19. Fit of model and data for viscosity over composition and temperature data.

CONCLUSIONS

The columns studied follow Darcy's law in the pressure drop relationship. Classic reduced velocity equations were evaluated and the Van Deemter function gave the least error. Transformation of the models reduces the error significantly, specifically, the log(h) versus $\sqrt{\nu}$ transformation on the Van Deemter model gave the least error. Viscosity relationships are highly non-linear and a preliminary transformation has been proposed.

ACKNOWLEDGMENTS

The authors thank Daiso® Corporation for sponsoring this work, Purdue University Grant No. 202435. The authors thank Mr. Kadoya and Mr. Matsutomi for discussions. We thank Water's Corporation and Eka Nobel Inc. for donation of the columns.

REFERENCES

1. Guiochon, G.; Felinger, A.; Shirazi, D.; Katti, A. *Fundamentals of Preparative and Non-Linear Chromatography, 2nd Edition*; Elsevier: Amsterdam, 2006; 257–264.

2. Hagen, G. Pogg. Ann. **1939**, *46*, 423–442.
3. Poiseuille, J. Comptes Rendus **1940**, *11*, 961–967.
4. Darcy, H. *Les Fontaines Publiques de la Ville de Dijon*, Dalmont: Paris, 1856.
5. Ergun, S. Anal. Chem. **1951**, *23* (1), 151–156.
6. Bernea, E.; Rednick, R. Chem. Eng. J. **1978**, *15*, 215–227.
7. Lin, H.; Horváth, Cs. Chem. Eng. Sci. **1981**, *36* (1), 47–55.
8. Katz, E.; Ogan, K.; Scott, R. J. Chromatogr. A **1983**, *260*, 277–295.
9. Martin, M.; Eon, C.; Guiochon, G. J. Chromatogr. A **1974**, *99*, 357–376.
10. Comiti, J.; Renoud, M. Chem. Eng. Sci. **1989**, *44* (7), 1539–1545.
11. Osborne, S.; Reynolds, J. Royal Soc. Phil. Trans. **1883**, *174*, 935–982.
12. Bird, R.; Stewart, W.; Lightfoot, E. *Transport Phenomena*, Wiley: NY, 1962.
13. Van Deemter, J.; Zuiderweg, F.; Klinkenberg, A. Chem. Eng. Sci. **1956**, *5*, 271.
14. Lapidus, L.; Amundson, N. J. Phys. Chem. **1952**, *56*, 984.
15. Martin, A.J.P.; Synge, R.L.M. Biochem J. **1941**, *35*, 1359.
16. Golay, M.J.E. In: *Gas Chromatography*; Desty, D.H., Ed.; Butterworths: London, 1958, 36.
17. Guiochon, G.; Guillemin, C. *Quantitative Gas Chromatography*; Elsevier: Amsterdam, 1988.
18. Jennings, W. *Gas Chromatography with Capillary Columns*; Academic Press: NY, 1980.
19. Kucera, P.; Guiochon, G. J. Chromatogr. **1984**, *283*, 1.
20. Giddings, J.C. *Dynamics of Chromatography*; M. Dekker: NY, 1965.
21. Horváth, Cs.; Lin, H. J. Chromatogr. **1978**, *149*, 43.
22. Knox, J.H. J. Chromatogr. Sci. **1977**, *15*, 352.
23. Tallarek, U.; Bayer, E.; Guiochon, G. J. Am. Chem. Soc. **1988**, *120*, 1494.
24. Rathore, A.; Sofer, G. *Process Validation in Manufacturing of Biopharmaceuticals: Guidelines, Current Practices, and Industrial Case Studies*; CRC Press: 2005.
25. Krull, I.S.; Swartz, M.E. J. Am. Chem. Soc. **1997**, *119* (40), 9590.
26. Wang, X.; Germansderfer, A.; Harms, J.; Rathore, A. Biotechnol. Prog. **2007**, *23*, 55–60.
27. FDA, R *Analytical Procedures and Methods Validation: Chemistry, Manufacturing, and Controls*; Federal Register (Notices) 65 (169), 52,776–52,777 (30 August 2000).
28. ''International Conference on Harmonization; Draft Guidance on Specifications: Test Procedures and Acceptance Criteria for New Drug Substances and Products: Chemical Substances,'' Federal Register (Notices) 65 (251), 83041–83063 (29 December 2000).
29. Zhou, D.; Liu, X.; Kaczmarski, K.; Felinger, A.; Guiochon, G. Biotech. Prog. **2003**, *19*, 945.
30. Felinger, A.; Boros, B.; Ohmacht, R. Chromatographia **2002**, *56*, S61.
31. Szabelski, P.; Kaczmarski, K.; Cavazzini, A.; Liu, X.; Van Horn, J.; Guiochon, G. J. Chromatogr. **2002**, *950*, 41.
32. Liu, X.; Szabelski, P.; Kaczmarski, K.; Zhou, D.; Guiochon, G. J. Chromatogr. **2003**, *988*, 205.
33. Reid, R.; Prausnitz, J.; Poling, R. *The Properties of Gases and Liquids,* 4th ed.; McGraw-Hill: NY, 1987.

34. Grunberg, L.; Nisson, A. Nature **1949**, *164*, 799.
35. Arrhenius, S. Zeitschrift fur Physikalische Chemie **1887**, *1*, 285.
36. Li, J.; Carr, P. Anal. Chem. **1997**, *69*, 2530.
37. Viswanath, D.; Ghosh, T.; Prasad, D.; Dutt, D.; Rani, K. *Viscosity of Liquids*; Springer: Netherlands, 2007, 407–442.
38. Colin, H.; Diez-Masa, J.; Czaykowska, T.; Miedziak, I.; Guiochon, G. J. Chromatogr. **1978**, *167*, 41.
39. Herráez, J.; Belda, R.; Soln, J. Chemistry **2004**, *33* (2), 117–129.
40. El Falllah, M.Z.; Guiochon, G. Biotechnol. Bioeng. **1992**, *39*, 877.
41. Billy, K.; Velayudhan, A. J. Chromatogr. A. **1998**, *796*, 195.
42. Whitley, R.; Zhang, X.; Wang, N.-H.L. AIChE J. **1994**, *40*, 1067.
43. Felinger, A.; Guiochon, G. J. Chromatogr. **1998**, *796*, 59.
44. Scheibel, E.G. Ind. Eng. Chem. **1954**, *46*, 1569.
45. Knox, J.; Scott, R. J. Chromatogr. **1983**, *282*, 297.
46. Nelder, J.; Mead, R. Comput. J. **1965**, *7*, 308.
47. Lagarias, J.; Reeds, J.; Wright, M.; Wright, P. SIAM J. Optimiz. **1998**, *9* (1), 112.

Received July 10, 2008
Accepted September 15, 2008
Manuscript 6376